# Calculation of Symmetric Vortex Separation Affecting Subsonic Bodies at High Incidence

D. Almosnino* and J. Rom†
*Technion—Israel Institute of Technology, Haifa, Israel*

**A method for calculating the longitudinal aerodynamic coefficients and the pressure distributions on a body at reasonably high angles of attack is presented. The body is represented by a combination of source elements and vortex-lattice elements, including separation of the vortices at increasing angles of attack. The method is self-consistent in that the body and the separated vortex wake are treated as an integrated interacting system. The location of the separation line can be included as an arbitrary input from experimental data or can be evaluated approximately by a pressure-dependent criterion. Calculated values of the aerodynamic coefficients and pressure distributions on cone-cylinder and ogive-cylinder bodies compare well, qualitatively and quantitatively, with experimental data, including simulation of the dependence on Reynolds number.**

## Nomenclature

$A$ = influence coefficient matrix
$b$ = vector
$C_D$ = induced-drag coefficient
$C_L$ = lift coefficient
$C_m$ = pitching moment coefficient about nose tip
$C_{NOR}$ = normal-force coefficient
$C_p$ = pressure coefficient
$d$ = maximum body diameter
$F$ = fixed part of influence coefficient matrix
$i,j$ = indices
$\ell$ = body length
$M$ = Mach number
$n$ = iteration number
$\hat{n}$ = vector normal to surface
$N_c$ = axial number of elemental panels for a part of the body
$N_S$ = circumferential number of elemental panels over half a body
$Re_d$ = Reynolds number based on diameter
$S_0$ = potential sources strength vector
$U$ = freestream velocity
$u,v,w$ = velocity disturbance Cartesian components
$v(x)$ = variable part of influence coefficient matrix
$x,y,z$ = Cartesian coordinates
$x$ = potential vortices strength vector [Eq. (2)]
$\alpha$ = angle of attack
$\Delta x$ = integration step size
$\epsilon$ = difference vector
$\theta$ = circumferential angle
$\rho_s$ = spectral radius of a matrix
$\| \ \|$ = norm of a matrix

*Subscripts*

$0$ = at $\alpha = 0$ deg
NOR = normal
ref = reference
max = maximum
$N$ = nose
$s$ = separation
$\infty$ = of the freestream

Received Oct. 28, 1981; revision received June 28, 1982. 

*Instructor, Department of Aeronautical Engineering. Presently NASA/NRC Research Associate, NASA Ames Research Center, Moffett Field, Calif. Member AIAA.

†Professor, Lady Davis Chair in Experimental Aerodynamics. Associate Fellow AIAA.

## I. Introduction

PREDICTING the nonlinear aerodynamic characteristics of wing-body configurations at high incidence in subsonic flow is one of the most demanding aerodynamic problems. The difficulty in these calculations is the mutual interaction between the configuration and its vortex wake, which is separated from the surface, rolling up in the flow, and forming a shape that is not known a priori. The vortex wake influences the pressure distribution, causing a nonlinear variation of the aerodynamic coefficients as the angle of attack is increased.

Since the beginning of the 1970's, several panel-type computation methods[1-14] that can be used to make reasonable predictions of the nonlinear behavior of lifting-surface configurations at high angles of attack have been developed. Some methods[5,7-9] also include a linear model for the presence of the body, using potential source panels distributed over the body surface, or in some cases[1,7,9] making use of quadrilateral vortex rings, as well as a combination of source and vortex elements.

However, the accuracy of the results of such combined methods is limited by the fact that even at rather low incidence (already at 5 deg) nonlinear characteristics that are due to vortex shedding from the surface of the body itself do occur. The pair of vortices shed from a slender body stays symmetric up to about $\alpha = 25$ deg, depending mainly on the slenderness ratio and on the shape of the nose.[15,16] This complex flow structure causes large differences between the measured aerodynamic coefficients of the body and those predicted by the linear theories.

The discrepancy between the calculated results that use a linear model for the fuselage and the experimental data is especially noted for integrated modern-type, low-aspect-ratio wing-body configurations and many missile configurations.

Some simplified methods can be used in efforts to predict the nonlinear aerodynamic coefficients of slender bodies using cross-flow assumptions.[17-19] However, the applicability of these methods is limited to cases that fit the simplifying assumptions, and additional data are needed if any reasonable results are to be achieved. A more advanced calculation is suggested by taking into consideration the two-dimensional development of the boundary layer and its separation on the body surface in the cross-flow plane.[20] These methods are very restricted because of the strong three-dimensional flow effects on the development of the boundary layer on the body at angles of attack.

In view of this partial review it seems that a good prediction of the behavior of a wing-body configuration depends on a proper model for the presence of the vortex flow emanating

from the body. The present method is self-consistent in that the body and its vortex wake are treated as an integrated interacting system, thus eliminating the need of any independent input, except for a criterion for determining the separation of the vortices from the body.

## II. Present Method of Calculation

The surface of the body is divided into elemental panels (Fig. 1); equal or unequal axial spacing may be used (Figs. 1 and 2). A horseshoe vortex is placed within each panel, its head at the one-quarter chord line of the panel (Fig. 1). The trailing vortices continue over the surface of the body to its aft portion and then cancel on the centerline, if the body is closed in its rear part. The trailing vortices may stay in the surface of the body, or may leave the surface in order to simulate vortex shedding from the body (Fig. 1). Because of the three-dimensional shape of the surface of the body, the trailing vortices are not parallel to each other, unlike the classic horseshoe vortex model. This fact poses some problems concerning the best location of the control points, since there is no theory to indicate which is the best location for the present case. Therefore, the same location is used as in the classic vortex lattice method, that is, each panel contains a control point at mid-three-quarter chord line of the panel, in order to fulfill the "no-penetration" boundary condition for the flow at that point (Fig. 1).

A set of potential point sources is distributed along the body axis of revolution when the body is axisymmetric, and source panels are used in cases in which the body is of any three-dimensional shape. The location of the point sources is such that their axial position coincides with that of the control points on the body surface, and their own control points coincide with the control points of the vortex lattice accordingly (Fig. 1).

In the first stage of calculation, the body is placed at zero incidence. The strength of the sources $S_0$, which describe approximately the thickness distribution of the body at zero incidence, is calculated using the no-penetration condition at the control points, meaning that the net flow through that point should be zero

$$A_0 \cdot S_0 = -\vec{U} \cdot \hat{n}_0 \tag{1}$$

Here, $A_0$ is the geometric influence-coefficient matrix calculated for unit strength sources at each control point. Such calculations have been performed since von Kármán first suggested this method for axisymmetric thickness distribution.[21] The same type of equation holds if source panels are to be used, but a different influence-coefficient matrix must be calculated in that case.

The body now undergoes an angle-of-attack transformation. A geometrical influence-coefficient matrix $A$ for the horseshoe vortices is calculated, and then the strength $x$ of the bound vortices may be calculated using the new boundary conditions of no-penetration of the flow, considering also the induced velocity of the previously calculated source field

$$Ax = -(\vec{U} \cdot \hat{n} - \vec{U} \cdot \hat{n}_0) \tag{2}$$

Note that the previous is a linear calculation, and that this procedure is fully justified by the nature of Laplace equation, which allows for any combination of potential sources and vortices (or doublets) for the description of the body at incidence. In such calculations, the strength of one type of element is prescribed and the strength of the other type of element is then calculated using the boundary conditions.

### Determination of the Separation Line

At this stage the computer program sets the points where vortex shedding should occur. This is done either by imposing the location of separation based on external empirical data or by using the results of calculations. The calculation program itself may be used to impose a separation criterion based on initial pressure distribution, by determining the vortex separation at the location of the minimum pressure coefficient, assuming that this flow cannot resist an adverse pressure gradient. The last choice is, of course, only a rough approximation, but it seems to yield reasonable results considering the fact that the body is divided into cells of finite size. It is known that the separation line is expected to be located close to the line of minimum $C_p$ values on the body; a comparison between those lines is presented in Fig. 2, where the separation line is calculated by the method of Ref. 20.

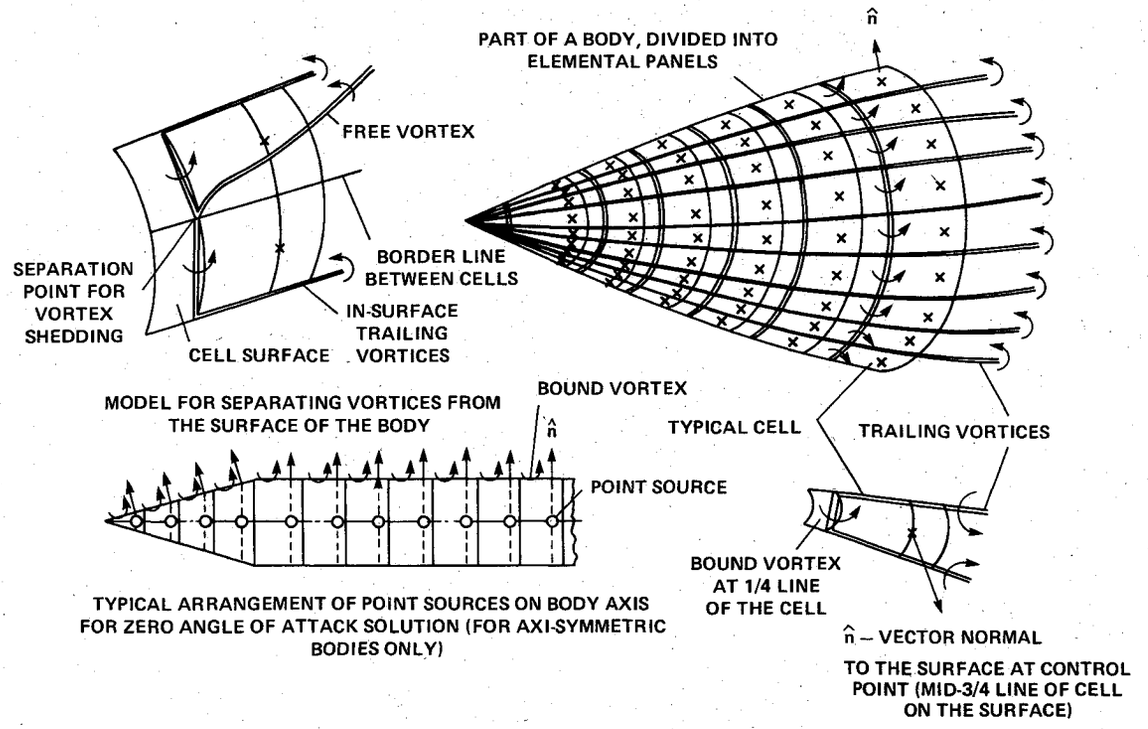


**Fig. 1 The model of the body in the present method, including the capability for vortex shedding.**

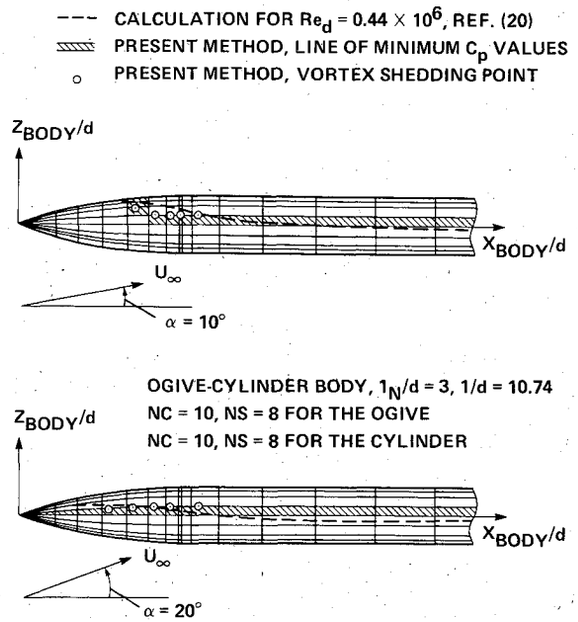


**Fig. 2 Position of separation of vortices from body as used in the present method.**

In order to carry on the inviscid calculation, some additional assumptions are required. The separation of the boundary layer from the body, which later forms the vortex cores, is dominated by the viscous-inviscid interaction between the boundary layer and the outer flow. Reynolds number has a most significant role in determining the position of this separation line. However, it is assumed that once the separation occurs, the resulting vortex wake may be treated by inviscid methods. It is also assumed that the separation zone is confined to a very narrow area (line) so that vortex shedding is concentrated at several points close to this line. (The method of shedding the vortices is described in Fig. 1.) The last assumption is supported (especially for slender bodies) by experimental results.[15,22-28]

### Calculation of the Vortex Wake

The position of the free vortices undergoes an iterative process at the end of which the vortices find their stationary position in space. This is done by dividing each line vortex into a finite number of segments and by imposing the boundary condition in the free wake; that is, the free vortex may not carry any forces. The new position of an edge point of a segment is calculated, in its turn, using a Euler-type integration process

$$y_i^{(2)} = y_{i-1}^{(2)} + \frac{v_{i-1}^{(2)}}{U + u_{i-1}^{(2)}} \Delta x_i \quad z_i^{(2)} = z_{i-1}^{(2)} + \frac{w_{i-1}^{(2)}}{U + u_{i-1}^{(2)}} \Delta x_i \qquad (3)$$

Here, $i$ is the index of the point to be moved (belonging to the segment $i$) and the superscripts $(2)$ and $(1)$ denote the new set and the old set of points, respectively. More accurate integration methods have been tried but it seems that their high cost in computer resources does not justify the additional marginal improvement in the accuracy of the results. The calculation starts from an initial guess for the shape of the line vortices. If there is no information on this shape it is found that linear conditions may be used successfully (starting from lines attached to the surface of the body). The common assumption of $\alpha/2$ initial vortex detachment angle may be inadequate for use in the case of three-dimensional bodies, leading to numerical problems.

An example of the calculated vortices paths appears in Fig. 3, where the paths of the free vortices over an ogive cylinder at $\alpha = 20$ deg are shown. This vortex pattern is very similar to

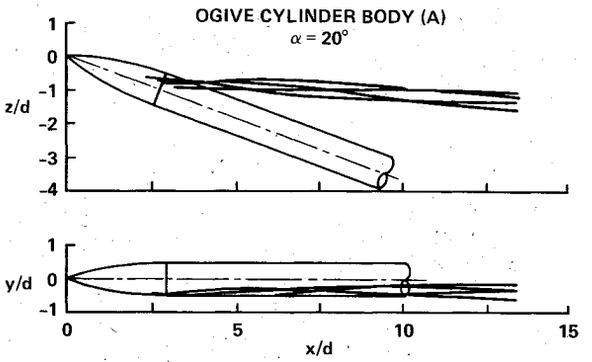


**Fig. 3 A typical example of the path of the free vortices (half-body) as calculated by the present method.**

that appearing in experimental flow-visualization photographs; however, it is too high above the body surface at its rear part. In reality, the flow about the base of the body may affect the actual position of the vortices at this region, but in the present calculation it is unaccounted for. Another reason for this behavior is the fact that the vortex wake that separates from the body is represented here by only four line vortices. An increase in the number of free vortices would cause a large increase in the computing time.

### Some Interesting Numerical Aspects

As described in the previous section, the process of calculation in the present method is a combination of two iterative cycles: a main cycle, from which the strength of the bound vortices is obtained, and an inner cycle for the calculation of the free vortices paths. The two cycles are strongly interconnected and interdependent.

Suppose that Eq. (2) is written simply as

$$Ax = b \qquad (4)$$

where $b$ is the right-hand side vector of Eq. (2). Matrix $A$ may be written as a combination of a constant part denoted by $F$, which is independent of the shape of the free vortices, and of a variable part denoted by $v(x)$. The last part depends on the geometrical shape of the free vortices representing the vortex wake. Although the values of $v(x)$ change from iteration to iteration, the function by which these values are calculated is unchanged in its form (Bio-Savart law[1]).

$$A = F + v(x) \qquad (5)$$

Equation (4) is then

$$[F + v(x)]x = b \qquad (6)$$

If one could know the shape of the wake and its exact representation by the vortex cores, then $v(x)$ would be known and Eq. (6) would give the final solution $x$ which approximates the vorticity distribution on the surface. It is assumed that such a solution exists and that it is unique.

Since the shape of the wake is unknown, the process of calculation is iterative, trying to get to the final solution $x$ together with the corresponding final matrix $v(x)$. The iterative process is

$$[F + v(x_n)]x_{n+1} = b \qquad (7)$$

where $x_n$ and $x_{n+1}$ are the solutions of iteration $n$ and $n+1$, respectively.

Subtraction of Eq. (6) from (7) gives

$$F\epsilon_{n+1} = -v(x_n)x_{n+1} + v(x)x \qquad (8)$$

where $\epsilon_{n+1}$ is the difference between the approximated solution $x_{n+1}$ and the final solution $x$.

If the initial guess for the free vortices path is close enough to the final solution, then it is possible to expand $v(x)_n$ to a series around $x$, using only the first approximation

$$v(x_n) = v(x+\epsilon_n) \simeq v(x) + \epsilon_n \frac{\partial v}{\partial x} \tag{9}$$

After replacing $v(x)$ in Eq. (8) by the last approximation, it follows that

$$[F+v(x)]\epsilon_{n+1} = -\epsilon_n \frac{\partial v}{\partial x}\epsilon_{n+1} - \epsilon_n \frac{\partial v}{\partial x}x \tag{10}$$

If convergence is assumed, then $\epsilon_{n+1} \ll x$, so that Eq. (10) may be written approximately

$$[F+v(x)]\epsilon_{n+1} \simeq -\epsilon_n \frac{\partial v}{\partial x}x \tag{11}$$

or

$$\epsilon_{n+1} \simeq -[F+v(x)]^{-1}\epsilon_n \frac{\partial v}{\partial x}x \tag{12}$$

and for $n+1$ steps

$$\epsilon_{n+1} \simeq \left[-(F+v(x))^{-1}x\frac{\partial v}{\partial x}\right]^{n+1}\epsilon_0 \tag{13}$$

where $\epsilon_0 = x_0 - x$ for the initial guess. It is well known[29] that the sufficient condition for convergence in such a case is

$$\left\|(F+v(x))^{-1}x\frac{\partial v}{\partial x}\right\| < 1 \tag{14}$$

or, alternatively,

$$\rho_s\left\{[F+v(x)]^{-1}x\frac{\partial v}{\partial x}\right\} < 1 \tag{15}$$

In some conditions[29] the sufficient condition for convergence is that for each iteration $n$

$$\left\|(F+v(x_n))^{-1}x_n\left(\frac{\partial v}{\partial x}\right)_n\right\| < 1 \tag{16}$$

However, these conditions demand that $x_n$ should be inside some radius of the final solution $x$; the difficulty is that this radius is unknown a priori. Although the lack of an existence and uniqueness theorem for the vortex-lattice methods strongly limits the last analysis, it seems that the last results give some important insight into the present method. This insight may prove useful in indicating some basic conditions for the success of the calculation. Equation (16) depends on $[F+v(x_n)]^{-1}$. The structure of the vortex lattice guarantees that $F$ is not ill conditioned. However, $v(x_n)$ may weaken this condition, since the free vortices may get close to a control point occasionally, and, thus, $[F+v(x_n)]$ may be ill conditioned. A possible (but costly) way to strength $[F+v(x_n)]$ is to increase the number of cells in the mesh. Increasing the number of cells strengthens $[F+v(x_n)]$ because the coefficients of $F$ depend inversely on their distance from the control points, so that a fine mesh increases the magnitude of these coefficients, especially on the main diagonal of $F$. On the other hand, $v(x_n)$ is not so strongly affected by an increase in the mesh size, while such an increase also means more control points where the boundary conditions are fulfilled, thus minimizing the chance of a free vortex to penetrate the surface.

The factor $(\partial v/\partial x)_n$ in Eq. (16) points out that the rate of convergence is increased when the initial guess for the free vortices paths is close to the final solution. A poor initial guess may lead to a diverging calculation, or increase the number of iterations required.

The last factor on which Eq. (16) is dependent is the solution vector $x_n$ itself. The magnitude of $x_n$ depends mainly on the angle of attack, and in many cases it increases even in a nonlinear manner as the angle of attack is increased. This indicates that the rate of convergence is slowing as the angle of attack is increasing. It is important in such a case to start from a good initial guess or to "build up" the calculation starting from low incidence, increasing the angle of attack gradually while using the previously calculated paths of free vortices as the initial guess for the increased angle of attack.

A typical behavior of the convergence of the main iterative process for the case of an ogive-cylinder body is presented in Fig. 4, where three to four iterations are sufficient for convergence with engineering accuracy. The points corresponding to $n=0$ in this figure are obtained for the linear initial solution (no separation).

### Calculation of the Aerodynamic Coefficients

Once the path of the free vortices is calculated, a new geometric influence coefficient matrix $A$ is recalculated, using the last calculated paths as the initial guess. The strength of the bound vortices $x$ is solved for, together with the aerodynamic coefficients and the new pressure distribution. The whole process repeats itself until convergence of the aerodynamic coefficients is achieved.

The pressure coefficient $C_{p_{ij}}$ is calculated for each cell $ij$ in the lattice, taking all contributing parts into consideration

$$C_{p_{ij}} = -\frac{2u}{U} - \frac{u^2+v^2+w^2}{U^2} \tag{17}$$

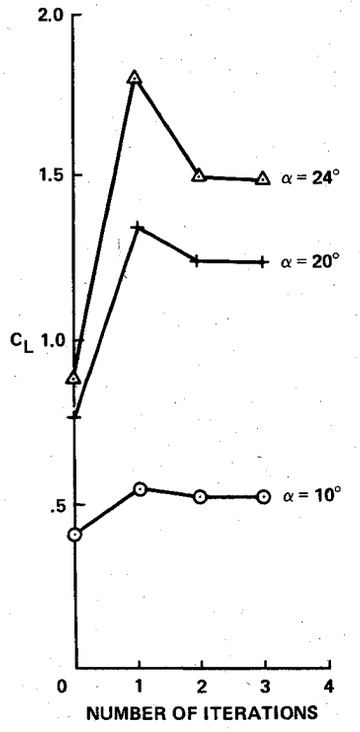


**Fig. 4 A typical convergence of the main iterative scheme for ogive-cylinder body (A).**

(Close-field velocity disturbance is obtained by conventional considerations,[1] assuming that each in-surface vortex is spread evenly within its corresponding element surface.)

Now the longitudinal aerodynamic coefficients are calculated by integrating the pressure coefficient over the body. Here the index $i$ runs for the total number of axial divisions, and the index $j$ runs for the number of circumferential divisions on half a body, due to the symmetry of the flow.

## III. Results

### Effect of Grid Spacing

The grid spacing has an effect on the magnitude and on the quality of the calculated pressure distribution. In the linear case (no vortex shedding along the body) there is almost no effect when the fineness of the mesh is increased over about 10 divisions axially and over 8 divisions circumferentially for the cylindrical part of an ogive cylinder body (A), of $\ell_N/d=3.0$, $\ell/d=10.74$ at $\alpha=20$ deg (Fig. 5). A clear improvement is obtained for the nose tip of the same body compared with the experimental data[30] at $x/d=0.5$, when the number of axial divisions is increased from 10 to 20, as a result of the improved capability to handle the large pressure gradient there (Fig. 6). Vortex shedding from a point farther downstream has almost no effect on the pressure at this station. In any case, the contribution of the pointed nose tip pressure to the overall aerodynamic coefficients is small. Results of the present method in the linear case are very similar to those obtained by a source-panel method for the same body (not presented here).

In the nonlinear case (with vortex shedding), the circumferential grid spacing has a more significant influence on the pressure distribution than in the linear case. This is demonstrated in Fig. 7 for $x/d=4.5$ over the same body at $\alpha=20$ deg, where using $N_S=16$ over half a body yields a better sensitivity of the pressure distribution to the vortex influence over the lee of the body than that obtained with

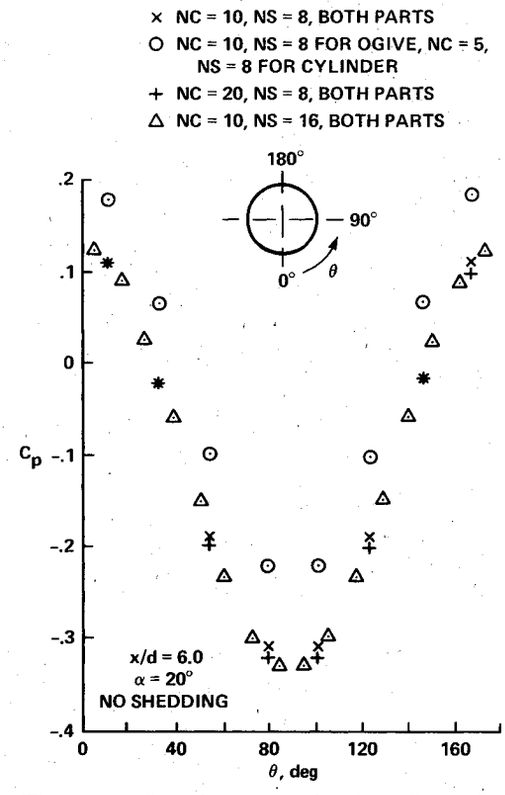


Fig. 5 The effect of mesh size on the circumferential pressure distribution, ogive cylinder (A) at $\alpha=20$ deg, no vortex shedding.

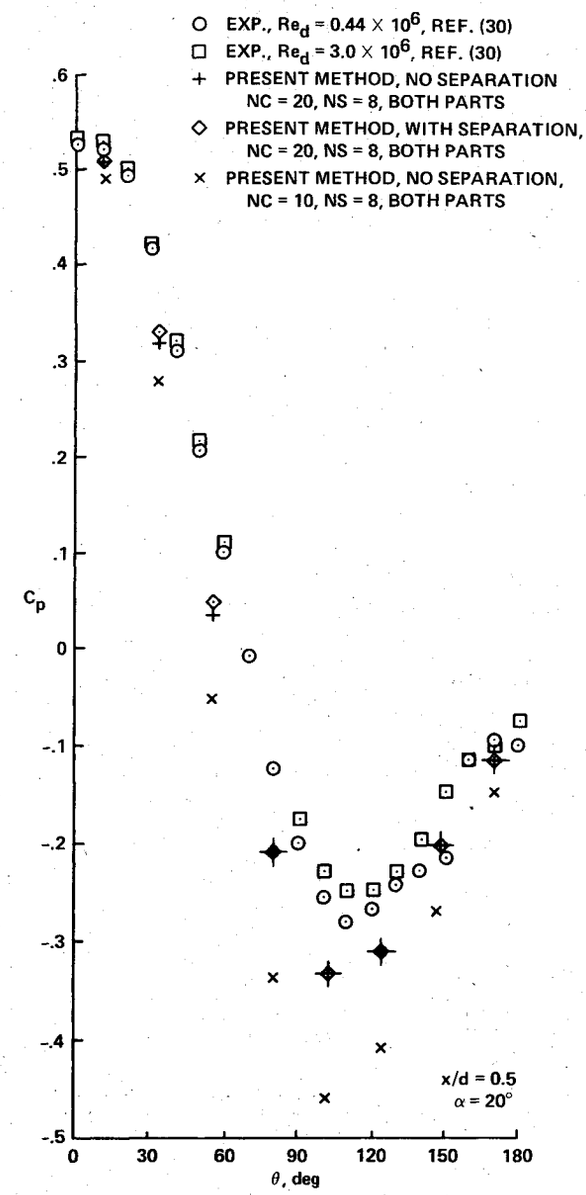


Fig. 6 The effect of mesh size on the circumferential pressure distribution near the nose tip of ogive cylinder (A).

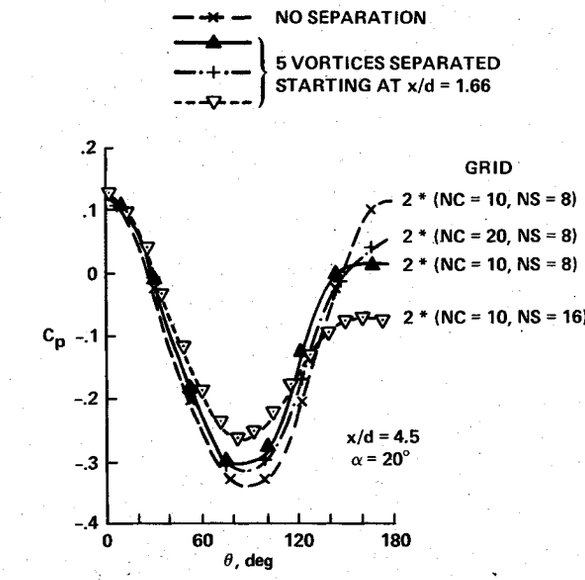


Fig. 7 Grid-size effect on the circumferential pressure distribution, ogive cylinder (A) with separation.

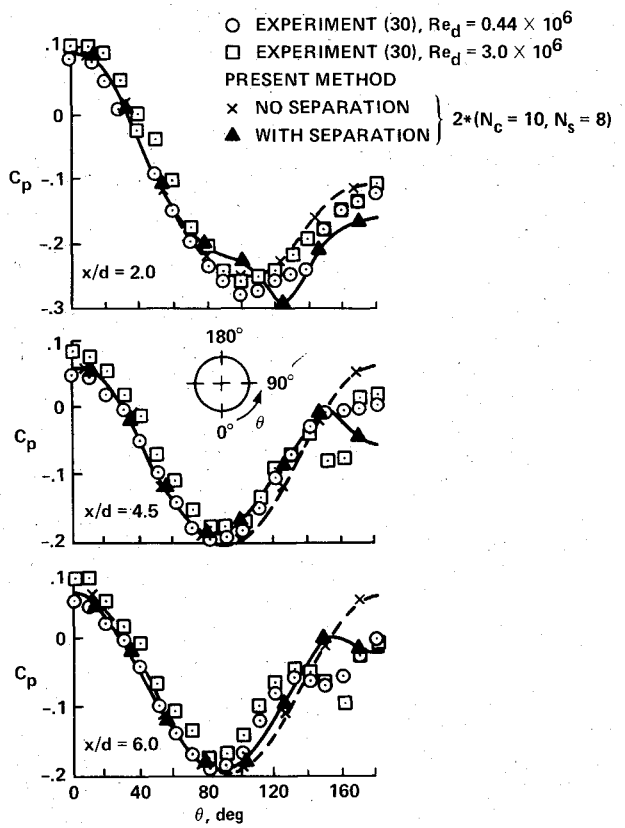


**Fig. 8 Circumferential pressure distribution over ogive-cylinder body (A) at $\alpha = 15$ deg.**

$N_S = 8$. Longitudinal spacing has less effect in the last case, possibly because the same number of vortices has been shed in all cases for the sake of equal comparison.

### Comparison with Experimental Data

The circumferential pressure distribution for a tangent ogive-cylinder body (A) of $\ell_N/d = 3.0$ and $\ell/d = 10.74$ is presented in Figs. 8 and 9 for $x/d = 2.0$, 4.5, and 6.0. The experimental data[30] are for $M = 0.3$ at $Re_d = 0.44 \times 10^6$ and at $Re_d = 3.0 \times 10^6$. At the lower incidence of 10 deg (not shown) the effect of the separated vortices is not strong, although some effects exist on the lee of the body.

At a higher incidence, the effect of vortex separation becomes stronger (Figs. 8 and 9 for $\alpha = 15$ and 20 deg). The difference between the separated solution and the non-separated one becomes more distinct at the aft stations of the body. The separated solution gives the right tendency of the curve, although not accurately. The reasons for this inaccuracy are the rough mesh size, inexact location of the separation points, and the small number of vortices shed from the body surface (four or five from the shoulder region). The last reason is probably responsible for the relatively too small influence of the calculated vortices at $x/d = 6.0$, together with a possible base effect at this station.

Although the present method is inviscid, it allows for various choices of the location of vortex shedding. As a result, a new pressure distribution is formed and together with it the total aerodynamic coefficients are influenced. Figure 10 shows the effect of moving the vortex-shedding locations on the total aerodynamic coefficients for $N_C = 10$ and $N_S = 8$ on both parts of the body. It can be seen that moving the initial separation from $x_S/d = 0.38$ to $x_S/d = 1.66$ has an effect similar to that of varying the Reynolds number from $3.0 \times 10^6$ to $0.44 \times 10^6$, respectively; however, the results should be interpreted with caution, since there is no exact information concerning the location of separation in this case.

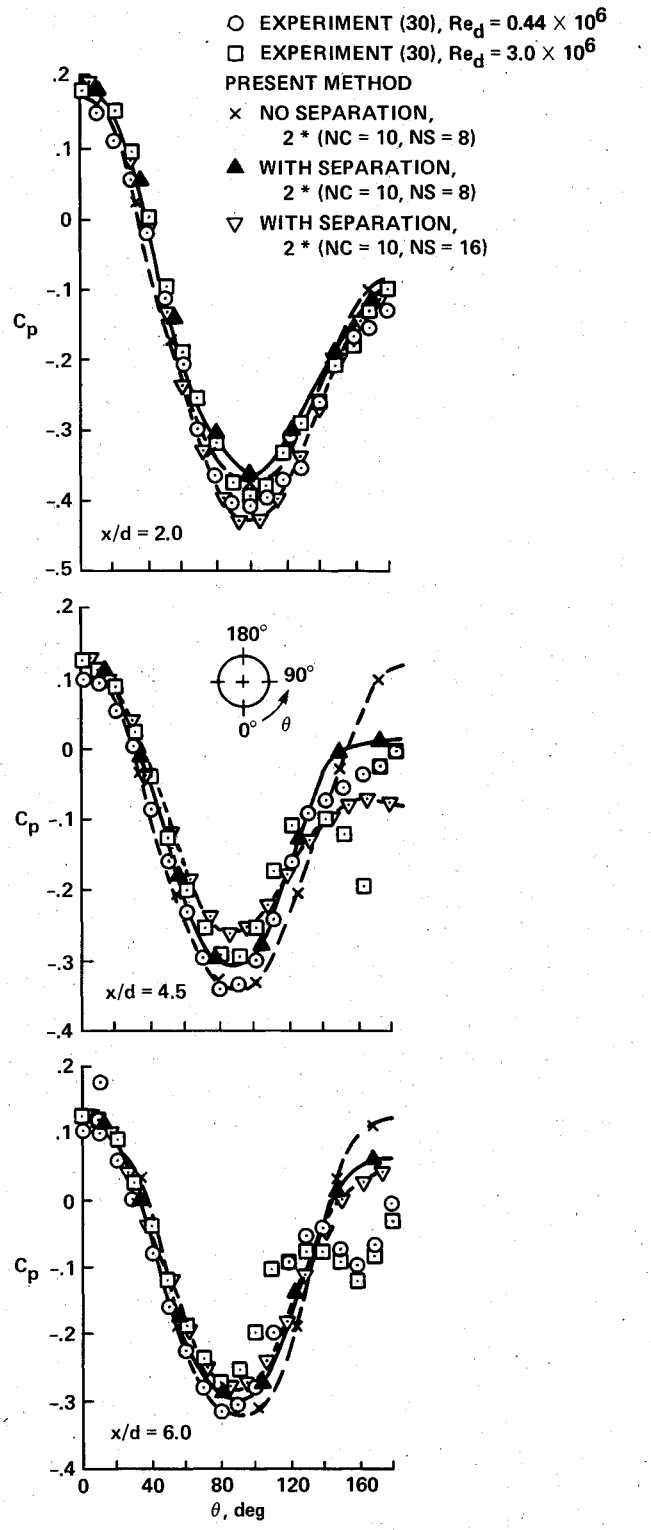


**Fig. 9 Circumferential pressure distribution over ogive-cylinder body (A) at $\alpha = 20$ deg.**

The absolute values of the pitching-moment coefficient are rather low (Fig. 10), which means that the influence of the calculated vortices in the near part is not strong enough. This may be explained by the lack of vortices separating from the aft portion and by the effect of the base flow, which is unaccounted for.

The circumferential pressure distribution for another ogive-cylinder body (B) with $\ell_N/d = 2.598$ and $\ell/d = 10.352$ is presented in Fig. 11. Using some empirical information about the separation in this case greatly improved the behavior of the calculated $C_p$ values for $\theta > 90$ deg at $\alpha = 20$ deg. The

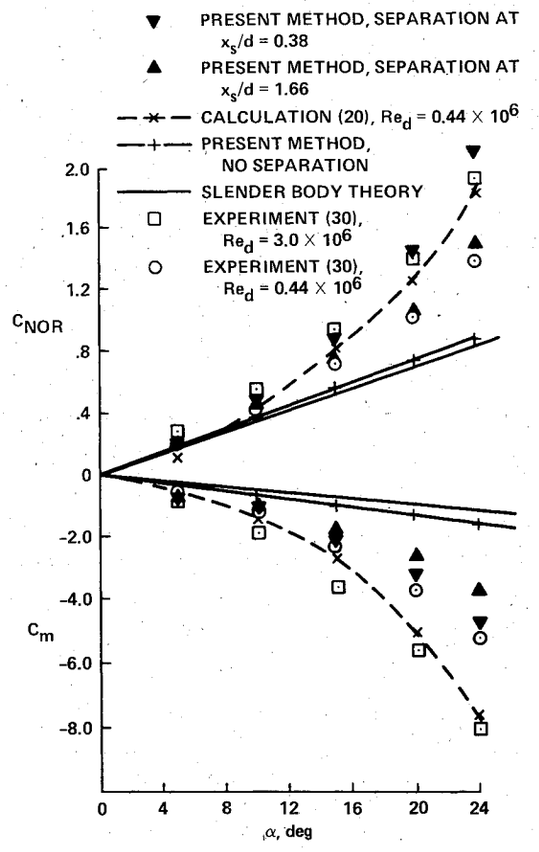


**Fig. 10 Normal-force and pitching-moment coefficients for ogive-cylinder body (A).**

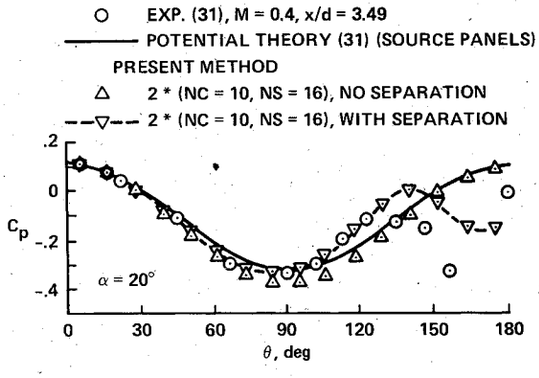


**Fig. 11 Circumferential pressure distribution over ogive-cylinder body (B).**

present method seems to give a better comparison with the experimental data than the vortex method of Ref. 31 (not presented in Fig. 11).

In the linear case the present method gives results similar to those obtained by a source-panel method,[31] but there is an unexplained mismatch at the region $\theta = 90$ deg where the present method gives higher absolute $C_p$ values.

The normal-force coefficient vs the angle of attack is presented in Fig. 12. Here too the nonlinear values of $C_{NOR}$ are much higher than those predicted by the slender body theory. The calculated results tend to match the higher Reynolds number experimental data.[32]

The total aerodynamic coefficients of a cone-cylinder body[33] with $\ell_N/d = 2$ and $\ell/d = 6.53$ are presented in Fig. 13. The behavior of the coefficients is similar to that reported before for the first case, including the low calculated absolute value of $C_m$.

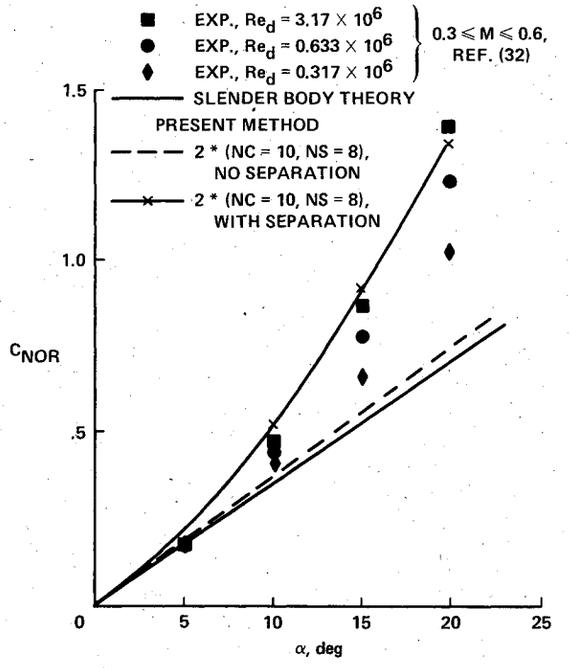


**Fig. 12 Normal-force coefficient for ogive-cylinder body (B).**

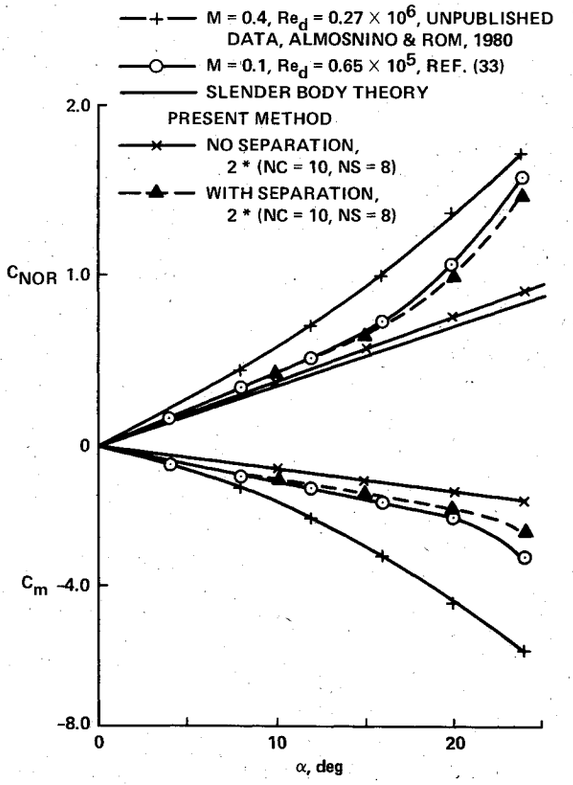


**Fig. 13 Normal-force and pitching-moment coefficients for a cone-cylinder body.**

Figure 14 gives the circumferential pressure distribution on a cone forebody. The experimental data[23] measured at $M = 0.6$ and the results calculated for $M = 0.0$ and 0.6 are compared using the Göthert similarity law. The calculated effect of the vortices is small because only one vortex was separated in this case. The results should be viewed with some caution since the separation position in the experimental data is located at 95% of the length of the cone, near its base; therefore, it is influenced by the base itself.

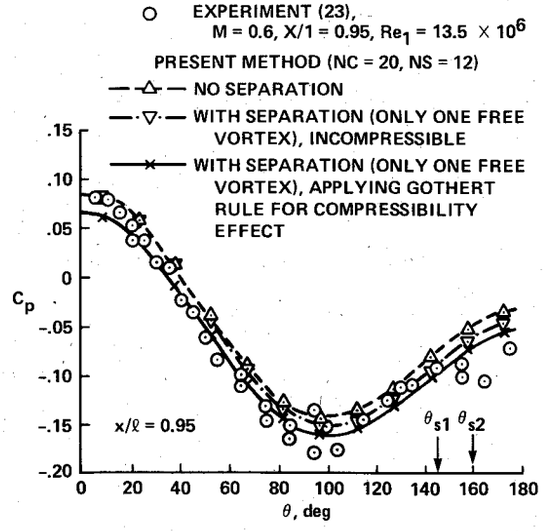


**Fig. 14 Circumferential pressure distribution over a slender cone forebody at $\alpha = 12.75$ deg.**

### Code Performance

At present, a typical solution for the bodies mentioned in the previous section would take about 3 min per iteration on an IBM 370/168 computer. This time is based on a grid of $N_C = 10$, $N_S = 8$ for each part of the body, separating five vortices from the surface, each including about 25 segments, and demanding a convergence ratio of 0.5% for the main iterative process. The computer time may vary largely, depending on the grid size selected, the number of free vortex lines, and the degree of accuracy demanded. The quality of the results depends on a good simulation of the vortex wake and its roll up. This can be achieved by increasing the number of vortices shed along the body, together with a better treatment of the roll up process. Recently published works may prove to be useful in this context.[34-36]

## IV. Discussion and Conclusions

A method for calculating the longitudinal aerodynamic coefficients and the pressure distribution on a body at high angles of attack is presented in this report. This method is self-consistent in that the body and the vortex wake, which is separated from the body, are treated as an integrated interacting system. The method is self-consistent also in that no outside independent input is required, except for determining the location of the separation line of the vortices that are shed from the body. This location of the separation line can be inserted by arbitrary predetermination based on independent calculation or experimental results or can be determined by a separation criterion such as position of minimum pressure coefficient or any other function of the pressure distribution on the body.

In the present method it was found that because of the limitation on the accuracy of the calculations imposed by the mesh size used, the simplified criterion of minimum $C_p$ as the position of the cell from which vortex separation occurs was sufficient. Utilizing this criterion enables a complete self-consistent computational program. The results for the ogive-cylinder and cone-cylinder models at angles of attack up to 25 deg clearly indicate that this method simulates well the pressure distributions over the body, even in the separated zones.

The other option of determining the separation line as an arbitrary input allows the simulation of effects of Reynolds number on the aerodynamic characteristics. Here we assume that the variation of the location of the separation line as a function of the Reynolds number is known from experimental measurements (or may be available in the future from a theoretical evaluation).

The combination of vortex elements and source/sink elements enables a fair calculation of the three-dimensional body aerodynamics, as shown in the cone-cylinder and ogive-cylinder cases. The characteristics of thick wings can be calculated by a similar method, opening the possibility of evaluating the aerodynamic characteristics of complete wing-body configurations with separated vortex flow.

## Acknowledgments

The research reported in this paper is supported in part by the U.S. Army under Grant DAERO-78-G119 and by U.S. Air Force Grant AFOSR-80-0064 through their European offices.

## References

[1] Maskew, B., "Calculation of the 3-D Potential Flow around Lifting Nonplanar Wings and Wing-Bodies Using a Surface Distribution of Quadrilateral Vortex Rings," Laughborough University of Technology, England, REpt. TT 7009, Sept. 1970.

[2] Weber, J. A., Brune, G. W., Johnson, F. T., Lu, P., and Rubbert, P. E., "A 3-D Solution of Flows Over Wings with Leading Edge Vortex Separation," NASA SP-347, 1975, pp. 1013-1032; also *AIAA Journal*, Vol. 14, April 1976, pp. 519-525.

[3] Smith, J.H.B., "A Theory of the Separated Flow from the Curved Leading Edge of a Slender Wing," RAE Tech. Note, Aero 2535, Nov. 1957.

[4] Johnson, F.T., Lu, P., Tinoco, E. N., and Epton, M. A., "An Improved Panel Method for the Solution of 3-D Leading Edge Vortex Flows," NASA CR-3278/3279, 1980.

[5] Johnson, F. T., "A General Panel Method for the Analysis and Design of Arbitrary Configurations in Incompressible Flows," NASA CR-3079, 1980.

[6] Kandil, O. A., Mook, D. T., and Nayfeh, A. H., "A Numerical Technique for Computing Subsonic Flow Past Three-Dimensional Canard-Wing Configurations with Edge Separation," AIAA Paper 77-1, Jan. 1977.

[7] "Vortex Lattice Utilization," Workshop held at NASA Langley Research Center, NASA SP-405, 1976.

[8] Atta, E. and Nayfeh, A. H., "Nonlinear Aerodynamics of Wing Body Combinations," AIAA Paper 78-1206, July 1978.

[9] Asfar, K. R., Mook, D. T., and Nayfeh, A. H., "Application of the Vortex Lattice Technique to Arbitrary Bodies," *Journal of Aircraft*, Vol. 16, July 1979, pp. 421-424.

[10] Rom, J. and Zorea, C., "The Calculation of the Lift Distribution and the Near Vortex Wake Behind High and Low Aspect Ratio Wings in Subsonic Flow," Dept. of Aeronautical Engineering, Technion, Haifa, Israel, TAE Rept. 168, Jan. 1973.

[11] Rom, J., Zorea, C., and Gordon, R., "On the Calculation of Non-Linear Aerodynamic Characteristics and the Near Vortex Wake," ICAS Paper 74-27, Aug. 1974.

[12] Zorea, C. and Rom, J., "The Calculation of Nonlinear Aerodynamic Characteristics of Wings and Their Wakes in Subsonic Flow," *Israel Journal of Technology*, Vol. 16, 1978, pp. 83-96.

[13] Almosnino, D., Zorea, C., and Rom, J., "A Method for Calculating Longitudinal Characteristics of Wings and Multiple Lifting Surfaces in Subsonic Flow and at High Angles of Attack," *Israel Journal of Technology*, Vol. 16, 1978, pp. 132-141.

[14] Rom, J., Almosnino, D., and Zorea, C., "Calculation of the Non-Linear Aerodynamic Coefficients of Wings of Various Shapes and Their Wakes, Including Canard Configurations," *ICAS Collection of Papers of the 11th Congress of ICAS*, Lisbon, Vol. 1, Sept. 1978, pp. 333-344.

[15] Mendenhall, M. R. and Nielsen, J. N., "Effect of Symmetrical Vortex Shedding on the Longitudinal Aerodynamic Characteristics of Wing-Body-Tail Combinations," NASA CR-2473, 1975.

[16] Nielsen, J. N., "Nonlinearities in Missile Aerodynamics," AIAA Paper 78-20, Jan. 1978.

[17] Angelucci, S. B., "A Multivortex Method for Axisymmetric Bodies at Angle of Attack," *Journal of Aircraft*, Vol. 8, Dec. 1971, pp. 959-966.

[18] Angelucci, S. B., "Multivortex Model for Bodies of Arbitrary Cross-Sectional Shapes," AIAA Paper 73-104, 1973.

[19] Fidler, J. E., "Approximate Method for Estimating Wake Vortex Strength," *AIAA Journal*, Vol. 12, May 1974, pp. 633-635.

[20]Marshall, F. J. and Deffenbaugh, F. D., "Separated Flow over Bodies of Revolution Using an Unsteady Discrete Vorticity Cross Wake," NASA CR-2414, 1974.

[21]von Kármán, T., "Calculation of the Flow Field around Airships," NACA TM-574, July 1930.

[22]Clark, W. H., Peoples, J. R., and Briggs, M. M., "Occurrence and Inhibition of Large Yawing Moments during High Incidence Flight of Slender Missile Configurations," AIAA Paper 72-968, Sept. 1972.

[23]Peake, D. J., Owen, K. F., and Higuchi, H., "Symmetrical and Asymmetrical Separations about a Yawed Cone," *High Angle of Attack Aerodynamics*, AGARD CP 247, Oct. 1978, pp. 16-1 to 16-27.

[24]Clark, W. C. and Nelson, R. C., "Body Vortex Formation on Missiles at High Angles of Attack," AIAA Paper 76-65, 1976.

[25]Thomson, K. D. and Morrison, D. F., "The Spacing Position and Strength of Vortices in the Wake of Slender Cylindrical Bodies at Large Incidence," Weapon Research Establishment, Salisbury, South Australia, Tech. Rept. NSA 25, June 1969; also, *Journal of Fluid Mechanics*, Vol. 50, Dec. 1971, pp. 751-783.

[26]Krouse, J. R., "Induced Side Forces on Slender Bodies at Angles of Attack and Mach Numbers of 0.55-0.80," Naval Ship Research and Development Center Rept. AL-79, Washington, D.C., May 1971.

[27]Pick, G. S., "Investigation of Side Forces on Ogive Cylinder Bodies at High Angles of Attack in the $M=0.5$ to 1.1 Range," AIAA Paper 71-570, June 1971.

[28]Clark, W. H., "Body Vortex Formation on Missiles in Compressible Flows," AIAA Paper 77-1154, Aug. 1977.

[29]Fröberg, C. E., *Introduction to Numerical Analysis*, 2nd ed., Addison Wesley, London, England, 1970.

[30]Tinling, B. E. and Allen, C. Q., "An Investigation of the Normal Force and Vortex Wake Characteristics of an Ogive-Cylinder Body at Subsonic Speeds," NASA TN D-1297, 1962.

[31]Sheffield, S. J. and Deffenbaugh, F. D., "A 3-D Vortex Wake Model for Missiles at High Angles of Attack," NASA CR-3208, 1980.

[32]Deffenbaugh, F. D. and Koerner, W. G., "Asymmetric Wake Development and Associated Side Force on Missiles at High Angles of Attack," AIAA Paper 76-364, July 1976.

[33]Rom, J. and Almosnino, D., "Investigation of Nonlinear Aerodynamic Characteristics of Slender Bodies at High Incidence in Subsonic and Transonic Speeds," Dept. of Aeronautical Engineering, Technion, Haifa, Israel, TAE Rept. 431, Dec. 1980.

[34]Kandil, O. A. and Balakrishnan, L., "Recent Improvements in the Prediction of the Leading and Trailing Edge Vortex Cores of Delta Wings," AIAA Paper 81-1263, June 1981.

[35]Hoeijmakers, H.W.M. and Vaatstra, W., "A Higher-Order Panel Method Applied to Vortex Sheet Roll-up," AIAA Paper 82-0096, Jan. 1982.

[36]Luckring, J. M., Schoonover, W. E. Jr., and Frink, N. T., "Recent Advances in Applying Free Vortex Sheet Theory for the Estimation of Vortex Flow Aerodynamics," AIAA Paper 82-0095, Jan. 1982.